

See discussions, stats, and author profiles for this publication at: <https://www.researchgate.net/publication/257581987>

On the dehydroindigo contribution to Maya blue. J Mater Sci

ARTICLE *in* JOURNAL OF MATERIALS SCIENCE · OCTOBER 2013

Impact Factor: 2.37 · DOI: 10.1007/s10853-013-7534-z

CITATIONS

13

READS

86

5 AUTHORS, INCLUDING:



[Antonio Domènech](#)

University of Valencia

282 PUBLICATIONS 3,715 CITATIONS

[SEE PROFILE](#)



[Francisco M Valle-Algarra](#)

University of Valencia

44 PUBLICATIONS 683 CITATIONS

[SEE PROFILE](#)



[Marcelo E Dómine](#)

Universitat Politècnica de València

55 PUBLICATIONS 1,422 CITATIONS

[SEE PROFILE](#)

On the dehydroindigo contribution to Maya Blue

Antonio Doménech-Carbó · María Teresa Doménech-Carbó · Francisco Manuel Valle-Algarra · Marcelo E. Domine · Laura Osete-Cortina

Received: 13 April 2013/Accepted: 13 June 2013/Published online: 25 June 2013
© Springer Science+Business Media New York 2013

Abstract A series of data from voltammetric, spectral, and UPLC–MS and Py–GC–MS analyses of extracts from synthetic Maya Blue-type specimens provides evidence on the presence of a significant amount of dehydroindigo, identified on the basis of its MS, FTIR, and UV–Vis signatures, accompanying indigo and other minority compounds, supporting the view of this material as a complex polyfunctional organic–inorganic hybrid material. Estimates of dehydroindigo/indigo in-depth distribution and thermochemical data for the dye association to the clay from chromatographic and voltammetric data are provided.

Introduction

Since its discovery by Merwin [1], the Maya Blue (MB), a pigment widely used in wall paintings, pottery, and sculptures by the Mayas and other ancient Mesoamerican cultures, has attracted attention because of its surprising durability, reflected in its enormous resistance to the attack of acids, alkalis, organic reagents, and biodegradation, and its characteristic hue [2, 3]. This attention is growing increasingly during the last decade due to the characteristic

of MB as a distinctive member of the so-called inorganic–organic hybrid materials [4].

Due to the absence of historical sources describing the preparation recipe of the pigment, the composition of MB became intriguing. In the 60s, Shepard [5] introduced the idea of MB resulting from embedding a dye to certain clays in Yucatan whereas Gettens [6] systematized acid attack tests for identifying MB and Van Olphen [7] described different procedures to prepare synthetic MB analogues from indigo with palygorskite and sepiolite. Currently, it is recognized that MB is a material resulting from the attachment of indigo (see Chart 1) or indigotin, 3H-indol-3-one-2-(1,3-dihydro-3-oxo-2H-indol-2-ylidene)-1,2-dihydro-(2E), a well-known blue dye [8] extracted from leaves of *añil* or *xiuquitlil* (*Indigofera suffruticosa* and other species), to the clay matrix of palygorskite, a fibrous phyllosilicate of ideal composition $\text{Si}_8(\text{Mg}_2\text{Al}_2)\text{O}_{20}(\text{OH})_2(\text{H}_2\text{O})_4 \cdot 4\text{H}_2\text{O}$. The strong attachment of the dye to the clay support can generically explain the stability of the pigment; however, the details on the nature of the indigo–palygorskite association, the location of the dye molecules on the clay support, and the origin of the color have remained controversial [9–27]. With regard to the location of indigo molecules on the clay support, it has been proposed that indigo molecules could anchor into the channels of palygorskite [5, 13, 15, 19, 24, 26], or to be adsorbed onto the external surface of the clay [7] or external truncated channels [25], or blocking the entrances at the edges of palygorskite channels [14, 26]. Different proposals have been made for the interaction between indigo and palygorskite, including formation of hydrogen bonds between the C=O and N–H units of the dye with edge silanol units of the clay [14], formation of hydrogen bonds between indigo carbonyls (and eventually NH units) and structural water [13, 15, 19], direct bonding between the clay octahedral Mg^{2+} and Al^{3+} cations and the dye molecules without water [24], and specific bonding to

A. Doménech-Carbó (✉) · F. M. Valle-Algarra
Departament de Química Analítica, Universitat de València,
Dr. Moliner, 50, Burjassot, 46100 Valencia, Spain
e-mail: antonio.domenech@uv.es

M. T. Doménech-Carbó · L. Osete-Cortina
Institut de Restauració del Patrimoni, Universitat Politècnica de
València, Camí de Vera s/n, 46022 Valencia, Spain

M. E. Domine
Instituto de Tecnología Química, ITQ, Universitat Politècnica de
València—CSIC, Avda. Los Naranjos s/n, 46022 Valencia,
Spain

Al^{3+} substituted Si^{4+} sites in tetrahedral centers [20, 22, 23]. The role of water evacuation–rehydration in MB has been discussed [26, 28].

The peculiarity of the color of MB is due not only to its characteristic brightness and blue-greenish hue, but also to its variability, ranging from a bright turquoise to a dark-greenish blue [2, 3]. Although the MB color was also attributed to Mie light dispersion due to iron and iron oxide nanoparticles detected in several pigment samples [10–12], there was general agreement in which the main effect responsible for the MB color was the bathochromic shift of the indigo absorption bands resulting from the dye attachment to the clay support [16–19].

In this context, examination of MB samples by means of voltammetry of microparticles, a solid state electrochemical methodology developed by Scholz and co-workers [29–31] which provides analytical information on sparingly soluble solids, supported by infrared (ATR–FTIR) and visible spectroscopies and microscopical analysis (SEM/EDX, TEM, AFM) prompted Doménech-Carbó et al. [32] to propose that: (i) dehydroindigo, one oxidized form of indigo, accompanies this dye in MB; (ii) the variation in the dehydroindigo/indigo ratio would determine the hue of the pigment and its characteristic variability. These ideas were consistent with thermochemical parameters calculated from voltammetric data and subsequent analysis of archeological MB samples and synthetic MB specimens [32–35]. Such results provide a view of MB as a polyfunctional hybrid inorganic–organic material where different dye molecules could be located in different clay sites thus defining different topological redox isomers [36, 37], in line with recently reviewed formulations of the chemistry and electrochemistry of microporous materials [38].

Consistently, the presence of dehydroindigo accompanying indigo in MB, and the above complex view of this

material, although has received support from spectral data [39, 40], has been occluded in much of recent literature [24–26, 41–43]. The lack of dehydroindigo detection obeys to the elusive nature of the involved species: dehydroindigo is difficult to prepare and it is formed under very definite conditions on attaching indigo to the palygorskite clay. As being one minority component in the MB system, the spectral signatures of dehydroindigo become obscured by those of the main component, indigo, when large indigo loadings are used (1–20 wt% [24–28, 41–43]). Possibly, the reluctance to discuss this hypothesis is also associated to the persistence of the ‘uniqueness paradigm’ where MB would appear as a material, prepared by means of a unique recipe, having a unique organic component: indigo, attached to the palygorskite clay by means of a unique type of binding. As already discussed [44], this view should be replaced by a more complex vision of MB as a polyfunctional hybrid material. In particular, analytical data on archeological MB samples suggest that: (a) other indigoid dyes accompany indigo in MB samples [45], namely, dehydroindigo [32–37] and indirubin [35, 37], (b) the Mayas could prepare ‘Maya-yellow’ pigments [46] and other materials combining the natural sources (vegetables, clays) of MB [47], and (c) the Mayas could use different preparation procedures for obtaining such pigments [32–35, 46, 47]. Consistently, specific zwitterions and/or altered trans-isomers of methyl red have been detected in the methyl-red/palygorskite hybrid material [48].

In this report, we present new evidences for the presence of dehydroindigo in MB samples based on separation of indigoid compounds via liquid chromatography, namely, high performance liquid chromatography with diode array detection (LC–DAD) and ultra pressure liquid chromatography coupled with mass spectrometry (UPLC–MS) from synthetic MB specimens, including one commercial formulation, accompanied by pyrolysis–silylation gas chromatography–mass spectrometry (Py–GC–MS), FTIR spectroscopy, UV–Vis spectrophotometry, and voltammetry data. A set of thermochemical data for the dye attachment to the clay and indigo–dehydroindigo interconversion and the in-depth distribution of such dyes in the clay crystals are estimated by combining chromatographic and voltammetric data.

Experimental

Reagents, reference products, and MB-like specimen preparation

Methanol, dimethylsulfoxide (Carlo Erba), hexamethyldisilazane (HMDS) (Sigma-Aldrich) (purity 99%). Indigo

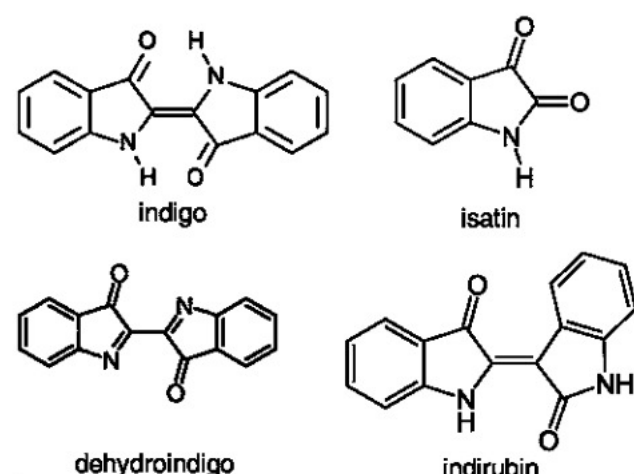


Chart 1 Representations of molecular structures of organic compounds in this study

(Fluka), isatin, (Aldrich), and indirubin (RG Chromadex) and commercial indigo pigment from *Isatis tinctoria* (Kremer 36000) were used as reference indigoid compounds. Dehydroindigo was prepared, following ‘hard’ oxidation procedure [49–51], by treating indigo with KMnO₄ in the presence of acetic acid and subsequent alkaline treatment of the intermediate diacetate. In order to mimic dehydroindigo formation under less exigent oxidizing conditions expected to operate in MB-type systems, a second dehydroindigo blank was prepared by means of a one-step ‘soft’ oxidation replacing permanganate by a Ca(OH)₂ plus PbO₂ aqueous suspension. The purple solid resulting from this soft oxidation process (labeled as SOIN sample) was actually a multicomponent system whose composition should incorporate dehydroindigo as a major compound.

Palygorskite, collected from the *Sak lu'um* classical site in Yucatan [32–36], was used to prepare MB-type specimens. These were prepared by finely grinding and mixing 1.0 % (w/w) indigo with palygorskite in an agate mortar and pestle during 60 min. The resulting specimens were separated in different portions (labeled as IN@P_i) and submitted to heating at temperatures between 120 and 180 °C in furnace during 24 h and subsequently were repeatedly rinsed with DMSO and acetone to remove indigo which remains unattached to the clay. In order to ensure minimal excess of non-associated indigo, the initial proportion of indigo to palygorskite (1 % w/w) in such samples was taken below the theoretical maximum of ca. 4 % w/w [52]. These conditions were selected within the suitable temperature interval where a previous kinetic study indicated reaction completion forming the indigo/dehydroindigo/palygorskite complex [53]. Commercial MB pigment (Kremer K36007) prepared from indigo and a siliceous matrix was also analyzed (IN@K). Blank experiments were also performed with palygorskite clay and indigo samples with no heating (IN@P).

Instrumentation and procedures

Aliquots of samples IN@K, IN@P, and the series of IN@P_i specimens were subjected to extraction with 1 mL of DMSO, 90:10 (v/v) H₂O:MeOH, and 50:50 (v/v) MeOH:DMSO mixtures in closed vials. Prior to the extraction the suspensions were maintained 24 h under magnetic stirring. The resulting extracts were studied conjointly with solutions of indigo, isatin, indirubin, and dehydroindigo in the same solvents.

The extracts were injected into a LC-DAD equipment consisted of an Agilent 1200 Series HPLC system equipped with a UV–Vis diode array detector set at 286 nm (Agilent Technologies, Palo Alto, CA, USA). The column was a Agilent Zorbax XDB C18 150 × 4.6 mm, 5 1 m particle

size (Agilent) preceded by a Agilent® Zorbax guard cartridge. Signals were processed by Agilent ChemStation software Ver. 10.02 [17–57]. Analysis was performed in the gradient mode. The mobile phase used was a mixture of two solvents (solvent A: water–0.1 % formic acid and solvent B: acetonitrile). Gradient conditions were initiated by holding the mobile phase composition for 0.1 min with 7 % B, after that it was changed linearly to 75 % B during 12 min. The composition was then changed to 98 % B in 3 min and maintained for 4.5 min as a cleaning step in order to improve the results. After cleaning, the eluent composition was returned to the initial 7 % B. The flow rate of the mobile phase was 1.2 mL/min and injection volume was 10 1 L. The column oven was operated at 35 °C.

UPLC–MS analyses of the extracts obtained from samples from the different reference materials and specimens were performed in an ACQUITY UPLC® system (Waters Corp.) with a conditioned autosampler at 4 °C. Liquid samples were prepared by diluting 0.1 mL of the extracts in 1.0 mL of acetonitrile. Typically, 20 1 L of the prepared sample was injected into the UPLC system equipped with Phenomenex Kinetex XB-C18 column (100 × 4.6 mm i.d.; 2.6 1 m particle size). The column temperature was maintained at 40 °C. The mobile phase, pumped at 1.0 mL/min, consisted of 0.1 % formic acid in water (A) and acetonitrile (B). The gradient applied was the following: 7 % B isocratic during 0.1 min, to 75 % B

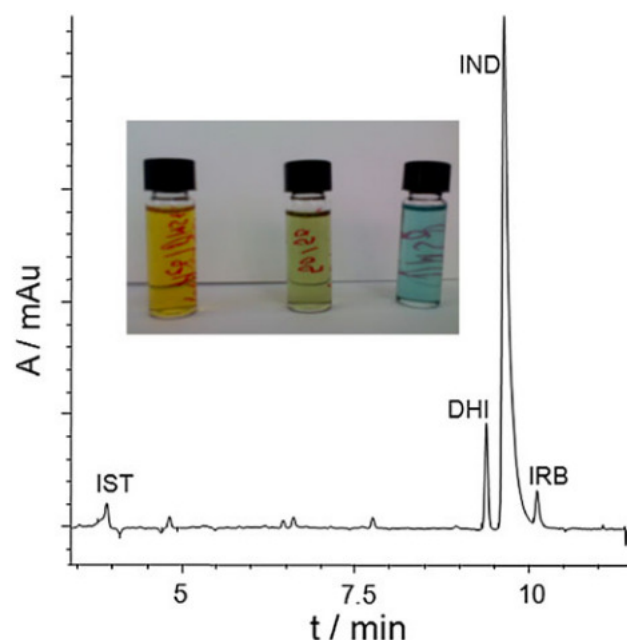


Fig. 1 LC–DAD chromatogram of indigo extract with DMSO from *Isatis tinctoria*. IND indigo, IRB indirubin, DHI dehydroindigo, IST isatin. Inset photographic images of the extracts of IN@K sample using, from left to right, 90:10 (v/v) H₂O:MeOH, 50:50 (v/v) MeOH:DMSO, and DMSO

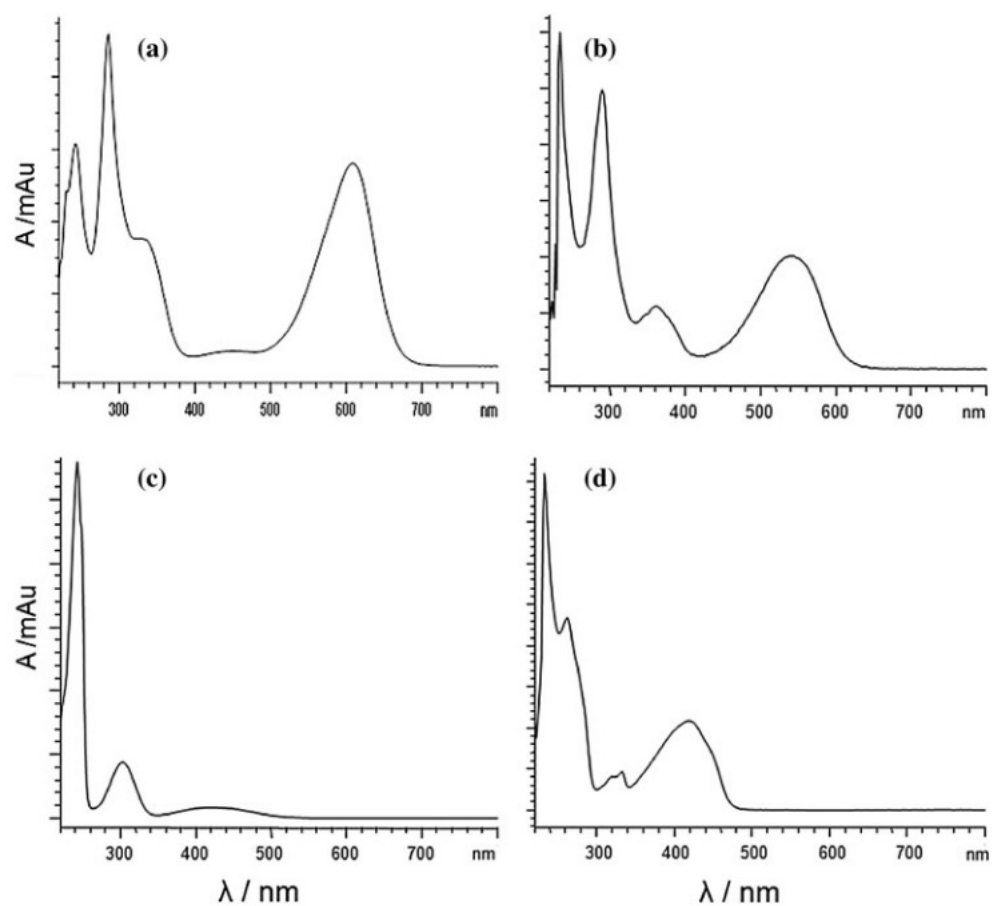
(linear) at 12 min, to 98 % B (linear) at 15 min, to 98 % B isocratic to 19.5 min, to 7 % B (linear) at 20.5 min and 7 % B isocratic until 25 min. Separated components of sample mixture were detected by means of a Waters ACQUITY™ XevoQToF Spectrometer (Waters Corp.) connected to the UPLC system via an electro-spray ionization (ESI) interface. The ESI source was operated in positive ionization mode with the capillary voltage at 1.5 kV. The temperature of the source and desolvation was set at 100 and 400 °C, respectively. The cone and desolvation gas flows were 100 and 800 L/h, respectively. All data collected in Centroid mode were acquired using Masslynx™ software (Waters Corp.). Leucine-enkephalin was used as the lock mass generating an $[M+H]^+$ ion ($m/z = 556.2771$) at a concentration of 2 ng/mL and flow rate of 50 1L/min to ensure accuracy during the MS analysis.

Py–GC–MS experiments were carried out with an integrated system composed of a CDS Pyroprobe 1000 heated filament pyrolyzer (Analytical Inc., New York, USA), and a gas chromatograph Agilent 6890 N (Agilent Technologies, Palo Alto, CA, USA) coupled to an Agilent 5973 N mass spectrometer (Agilent Technologies) and equipped with pyrolysis injection system. A capillary column HP-5MS (5 % phenyl–95 % methylpolysiloxane, 30 m, 0.25 mm i.d.,

0.25 1 m film thickness (Agilent Technologies) was used in order to provide the adequate separation of components. Pyrolysis was performed at 600 °C for 10 s using a precalibrated Pt coil-type pyrolyzer (CDS pyroprobe). The pyrolyzer interface and the inlet were set at 250 °C. The samples were injected in split mode (split ratio 1:40).

The chromatographic conditions were as follows: initial temperature of 50 °C held for 10 min and then increased at 5 °C/min up to 300 °C held for 8 min. Helium gas flow was set at 1.5 mL/min. The inlet pressure of the carrier gas was 89.1 kPa. The electronic pressure control was set to constant flow mode with vacuum compensation. Ions were generated by electron ionization (70 eV). The mass spectrometer was scanned from m/z 20 to m/z 800, with a cycle time of 1 s. An Agilent Chemstation software G1701CA MSD was used for GC–MS control, peak integration, and mass spectra evaluation. Tuning of the mass spectrometer was checked using perfluoro-tributylamine. EI mass spectra were acquired by total ion monitoring mode. The temperatures of the interface and the source were 280 and 150 °C, respectively. Wiley Library of Mass Spectra and NIST were used for identifying compounds. Samples were placed in a micro-quartz pyrolysis tube and then two small portions of quartz wool were introduced in both sides of the

Fig. 2 UV–Vis spectra of the compounds eluted in the LC system. **a** Indigo, **b** indirubin, **c** isatin, **d** dehydroindigo



quartz tube in order to avoid undesirable displacements of the sample and, after this, 5–10 mL of HMDS were added. Afterwards, the sample was placed in the pyrolysis coil and introduced in the pyrolysis interface. At ca. 1 g of solid sample of each reference material and specimens was introduced in a quartz tube with a small plug of quartz wool and 1 mL of HMDS was afterwards added.

Voltammetry of microparticles experiments were performed at sample-modified paraffin-impregnated graphite electrodes (PIGEs, [25, 26]) using a CH I660 equipment. A standard three-electrode arrangement was used with a platinum auxiliary electrode and a Ag/AgCl (3 M NaCl) reference electrode in a cell at 298 K. Experiments in aqueous media were performed with 0.50 M acetic acid/sodium acetate solutions at pH 4.75. For modified electrode preparation, ca. 0.5 mg of the samples were thoroughly powdered in an agate mortar and pestle and extended forming a spot of finely distributed material. The lower end of the graphite electrode was pressed over that spot of sample to obtain a sample-modified surface, as previously described [31–36].

ATR–FTIR spectra of sample-modified electrodes were obtained with a Bruker Vertex 70 Fourier-transform infrared spectrometer with an FR-DTGS (fast recovery deuterated triglycine sulfate) temperature-stabilized coated detector and an MKII Golden Gate Attenuated Total Reflectance (ATR) accessory. A total of 32 scans were collected at a resolution of 4 cm^{-1} and the spectra were processed using the OPUS/IR software. UV–Vis absorption spectra of the liquid extracts and diffuse reflectance spectra of powdered samples were obtained with a Perkin-Elmer lambda35 spectrometer, slit width 2 nm, scan speed 240 nm/min.

Results and discussion

Characterization of indigoid compounds and extraction experiments

A series of common extraction protocols were applied to all tested materials. Figure 1 shows the photographic images of the extracts of the IN@K sample with different solvent mixtures. The extract with $\text{H}_2\text{O}:\text{MeOH}$ (90:10, v/v) shows orange color while the extract with $\text{MeOH}:\text{DMSO}$ (50:50, v/v) is pale yellow and the extract with DMSO becomes blue. The UV–Vis spectra of the extracts agree well with the spectra of isatin, dehydroindigo, and indigo/indirubin, respectively, in the above mixtures of organic solvents, thus denoting that such components were present in the original sample. Figure 2 permits to compare the UV–Vis spectra for the above compounds eluted in the HPLC–DAD instrument. Such spectra are essentially

identical to those recorded, using the same solvent mixture, for indigo, indirubin, isatin, and dehydroindigo, respectively. Indigo absorption maximum in the visible region was located at 610 nm, whereas for dehydroindigo the maximum was placed at 445 nm, in agreement with literature data [39, 50, 54]. Spectrum of isatin produced a maximum at 300 nm, according to reported data [55], while indirubin displayed a maximum of absorption at 550 nm, also in agreement with literature [54, 56, 57]. Similar results were obtained for extracts from the IN@K sample, thus suggesting the presence of dehydroindigo and isatin accompanying indigo in this commercial formulation. Obviously, extraction experiments only provide information on major products, so that separation experiments via chromatographic procedures was carried out.

Figure 3 compares the ATR–FTIR spectra of SOIN sample, indigo and isatin in the 1500–1800 cm^{-1} wave-number region. In agreement with extensive literature data [58–60], indigo yields three overlapping signals at 1625 ($\text{dC-C}_{\text{ring}}$, nC-C , nC-H), 1600 and 1584 cm^{-1} (nC=C , nC=O , dN-H and dN-H , dC-H , $\text{dnC-C}_{\text{ring}}$), whereas isatin produces bands at 1726 and 1612 cm^{-1} , attributable to combinations of different C=O vibrations. As expected, the spectrum of SOIN sample contains features attributable to the superposition of the spectra of indigo and isatin, but several new significant bands appear. In Fig. 3, bands at 1692 and 1593 cm^{-1} , both absent in the spectra of indigo and isatin, are recorded. The first band can be attributed to C=O stretching while the second could correspond to the C=N stretching, characteristic of imines [61]. Examination of ATR–FTIR spectra of SOIN specimen revealed the vanishing of bands at ca. 3265 and 3200 cm^{-1} , which can

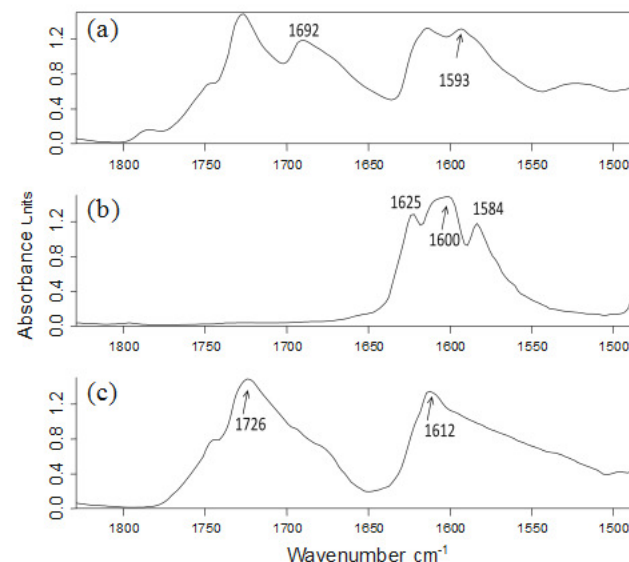


Fig. 3 ATR–FTIR spectra of: **a** synthetic indigo, **b** SOIN sample, and **c** isatin

be assigned to different types of intra- and intermolecular hydrogen bonds (N–H···N stretching vibrations of secondary amine), as well as the occurrence of a shoulder at about 3770 cm^{-1} , corresponding to the ‘free’ N–H band [62, 63]. These features, typically observed in azomethines and ketimines [64], appear in the spectra of indigo and isatin. Similarly, indigo exhibits bands at 1460 and 1483 cm^{-1} , both attributed to $\delta\text{C–C}$, $\delta\text{N–H}$, $\epsilon\text{C–C}_{\text{ring}}$ vibrations, vanish for SOIN sample.

Chromatography and mass spectra

Figure 4 shows the pyrograms obtained in the analysis of the studied materials by pyrolysis–silylation–gas chromatography–mass spectrometry using HMDS as derivatization reagent. This derivatization reagent has been selected due to the significant reduction in the number of by-products formed during the pyrolysis step if compared with commonly used methylation reagents such as tetramethyl ammonium hydroxide [65–67]. As it can be seen, the pyrogram of dehydroindigo (SOIN) is dominated by peaks at 19.92, 29.44, and 35.04 min that correspond to the TMS ether of benzyl alcohol (6), TMS ester of 2-amino benzoic acid (anthranilic acid, TMS ester) (12), and TMS ester of *N*-acetyl anthranilic acid (15), respectively. TMS derivative of anthranilic acid is the main compound present in isatin, accompanied by 1*H*-benzimidazole (9) (23.29 min), 1*H*-indole-2,3-dione (14) (34.54 min), and TMS ester of *N*-acetyl anthranilic acid (15). In contrast, pyrogram of synthetic indigo is dominated by peaks of aniline (3) (12.39 min), 1*H*-indole (10) (24.16 min) accompanied by TMS ester of benzoic acid (8) (22.79 min), and TMS ester of anthranilic acid. These last results are in good agreement with the studies previously reported on analysis of indigo pigments by Py–silylation–GC–MS [66, 67]. On the other hand, these results put in evidence the different behavior of these three indigoid compounds when subjected to thermal treatment as consequence of their different molecular structure. This differentiated pyrolytic behavior can be used here for detecting the presence of these three compounds in samples of MB-like specimens. Thus, 1*H*-indole could be used as marker compound of indigo molecules as this compound is scarcely found in pyrograms of dehydroindigo and isatin. More interestingly, TMS ether of benzyl alcohol can be used as marker compound of dehydroindigo as this compound only occurs in dehydroindigo pyrogram and is extensively formed in the experimental conditions applied in the present study.

Table 1 summarizes the main compounds identified in the series pyrograms of the three reference products and the two MB-like specimens studied (IN@P₁₅₀ and IN@K) with indication of the main fragment ions that characterize their mass spectra. In particular, the mass spectrum of the TMS

ether of benzyl alcohol, the selected marker compound for dehydroindigo, is characterized by the presence of the molecular ion at m/z 180 and by the fragment ion at m/z 165, that corresponds to the loss of a OTMS group followed by protonation [M–OTMS+H^+]. The fragment ion at m/z 135 is obtained by loss of three methyl groups [M–3Me^+] whereas the fragment ion [C_7H_7^+], that appears at m/z 91, is characteristic of a-cleavage of the benzyl bond in phenylalkanes. This ion further dissociates by successive loss of ethyne (acetylene), C_2H_2 , yielding the typical series of m/z 77, 65, 51, 39 [68].

Figure 4 also shows the pyrogram corresponding to MB-like specimen IN@P₁₅₀ in which both marker compounds (TMS ether of benzyl alcohol and 1*H*-indole) corresponding to dehydroindigo and indigo are unambiguously identified by their specific retention time and mass spectra. Similar result was found in the commercial MB-like pigment IN@K. Interestingly, in the latter, a strong peak at 13.60 min, which dominates the pyrogram, is identified as the TMS ester of boric acid. This compound has been associated with borax and other salts of boric acid, which are typical fluxes added to the silica to lower its melting point when the latter is used for preparing glazes. This result suggests that a more complex siliceous matrix has been used in the commercial MB pigment instead of palygorskite clay.

In order to unambiguously identify indigoid compounds extracted from reference products and samples from MB-like specimens, UPLC–MS analyses were performed. Chromatograms of indigo from *Isatis tinctoria*, isatin, dehydroindigo, and SOIN sample (dehydroindigo with minor amounts of indigo and isatin) in the UPLC–MS system are shown in Fig. 5. Isatin is the most polar component, appearing at 4.90 min, while indigo peak appears at 11.86 min under the same chromatographic conditions. In these conditions, dehydroindigo is eluted at 10.62 min. It is interesting to remark that, in the SOIN specimen, the

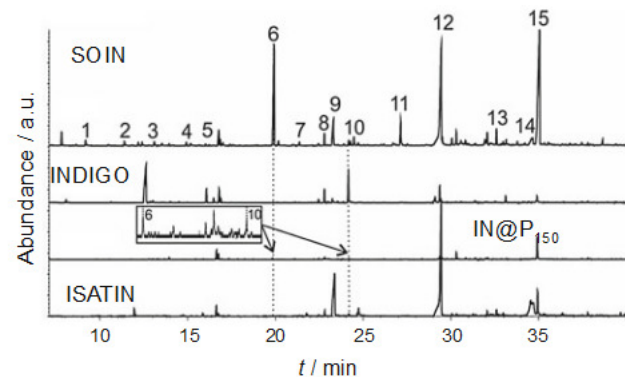


Fig. 4 Pyrograms corresponding to Py–GC–MS with HMDS of the reference products SOIN, indigo, and isatin and the heated MB specimen IN@P₁₅₀

Table 1 Main compounds identified by Py-GC-MS in samples of SOIN (dehydroindigo), indigo, isatin, IN@P₁₅₀, and IN@K together with molecular weight, retention time, and main fragment ions present in their mass spectra (relative abundance in brackets)

Ref.	Compound	<i>t</i> _r (min)	<i>M</i> _w	<i>m/z</i> ion fragments	SOIN	Indigo	Isatin	IN@P ₁₅₀	IN@K
1	<i>N</i> -Trimethylsilylacetamide	9.18	131	75(98), 116(100), 131(8)	+	–	–	–	–
2	Benzaldehyde	11.38	106	51(50), 77(100), 105(86), 106(86)	+	–	–	tr	–
3	Aniline	12.39	93	66(32), 93(100)	+	+++	+	+	tr
4	Benzyl alcohol	15.15	108	51(25), 79(100), 108(98)	+	–	–	–	–
5	Phenol, TMS ether	16.02	166	151(100), 166(40)	+	+	–	–	–
6	Benzyl alcohol, TMS ether ^a	19.92	180	91(100), 165(82), 135(70)	+++	–	–	+	tr
7	<i>N</i> -Trimethylsilylaniline	21.36	165	73(7), 150(100), 165(62)	+	+	tr	tr	tr
8	Benzoic acid, TMS ester	22.79	194	77(46), 105(75), 135(36), (179)100	++	++	+	+	+
9	1 <i>H</i> -Benzimidazole	23.29	118	63(16), 91(32), 118(100)	++	+	++	–	tr
10	1 <i>H</i> -Indole ^b	24.16	117	63(16), 90(40), 117(100)	–	+++	–	tr	–
11	4 <i>H</i> -3,1-Benzoxazin-4-one, 2-methyl	27.13	161	90(24), 119(28), 146(68), 161(100)	++	+	–	tr	–
12	2-Aminobenzoic acid, TMS ester	29.44	209	92(56), 120(100), 194(94), 209(70)	+++	++	+++	+	+
13	Benzoic acid, 2-(trimethylsilyl) amino-trimethylsilyl ester	32.59	281	73(71), 266(100), 281(6)	+	tr	+	tr	tr
14	1 <i>H</i> -Indole-2,3-dione	34.54	147	64(34), 92(75), 119(100), 147(65)	+	–	++	tr	–
15	<i>N</i> -Acetyl-2-aminobenzoic acid, TMS ester	35.04	251	119(72), 194(100), 209(72), 251(26)	+++	+	++	+++	+++

^a Marker compound of dehydroindigo, ^b marker compound of indigo

dehydroindigo peak is accompanied by weaker peaks for isatin and indigo and other minor components, thus denoting that, under the soft oxidizing treatment of indigo used to prepare such sample, other secondary products are formed. It is also pertinent to remark that non-heated indigo as well as non-heated indigo plus palygorskite mixture do not show comparable results, extraction/chromatographic experiments resulting almost exclusively in indigo peaks, with no dehydroindigo traces. This means that, in agreement with preliminary reports [32–37], dehydroindigo (and other compounds resulting from indigo oxidation) would be formed during heating indigo-palygorskite mixtures, the loss of clay's zeolitic water being the first step in such process [53].

The corresponding mass spectra of indigo, isatin, and dehydroindigo, recorded during UPLC-MS experiments on extracts from isatin and indigo reference products and dehydroindigo are shown in Fig. 5b. Under our experimental conditions, the signal for the molecular ion provides the $[M+H]^+$ mass which for indigo yields the main component at *m/z* 263.08 while for isatin is 148.04 and for dehydroindigo main component is recorded at *m/z* 261.06 (Table 2).

The relevant point to emphasize is that dehydroindigo appears as a ubiquitous component in all MB-type samples prepared from indigo and palygorskite, as well as in commercial formulation prepared from indigo and an unspecified silicate (sample IN@K). The corresponding chromatograms are shown in Fig. 6 for sample IN@K

(Fig. 6a) and IN@P₁₅₀ (Fig. 6b). In both cases, dehydroindigo accompanies indigo, as confirmed by the mass spectra shown in Fig. 6c, d, corresponding to the *m/z* region of the molecular ion of such compounds. The most intense signals are, as in experiments with the corresponding reference compounds, those at *m/z* 261.06 and 263.05. It should be noted that in the above MB-type samples, other minor organic components appear, as clearly indicated in chromatograms in Fig. 6a, b. This confirms our previously exposed idea that MB can be viewed as a polyfunctional organic-inorganic hybrid material rather than a binary indigo-palygorskite complex [36, 37, 44].

Electrochemistry

Figure 7 shows square wave voltammograms of indigo and isatin reagents and samples IN@K and SOIN attached to PIGEs in contact with aqueous acetate buffer, pH 4.75. As previously reported [32–37], indigo (Fig. 7a) displays two well-defined peaks at +0.45 and –0.30 V vs. Ag/AgCl. The first peak corresponds to the oxidation of indigo ($C_{16}H_{10}O_2N_2$) to dehydroindigo ($C_{16}H_8O_2N_2$) while the second can be attributed to the reduction of indigo to leucoindigo ($C_{16}H_{12}O_2N_2$). Voltammograms of indigo from vegetables show additional peaks due to minor compounds [69]. Isatin produces a main reduction peak at ca. –0.55 V (Fig. 7b) that can be described in terms of the two-proton, two-electron reduction of the carbonyl group at position 3

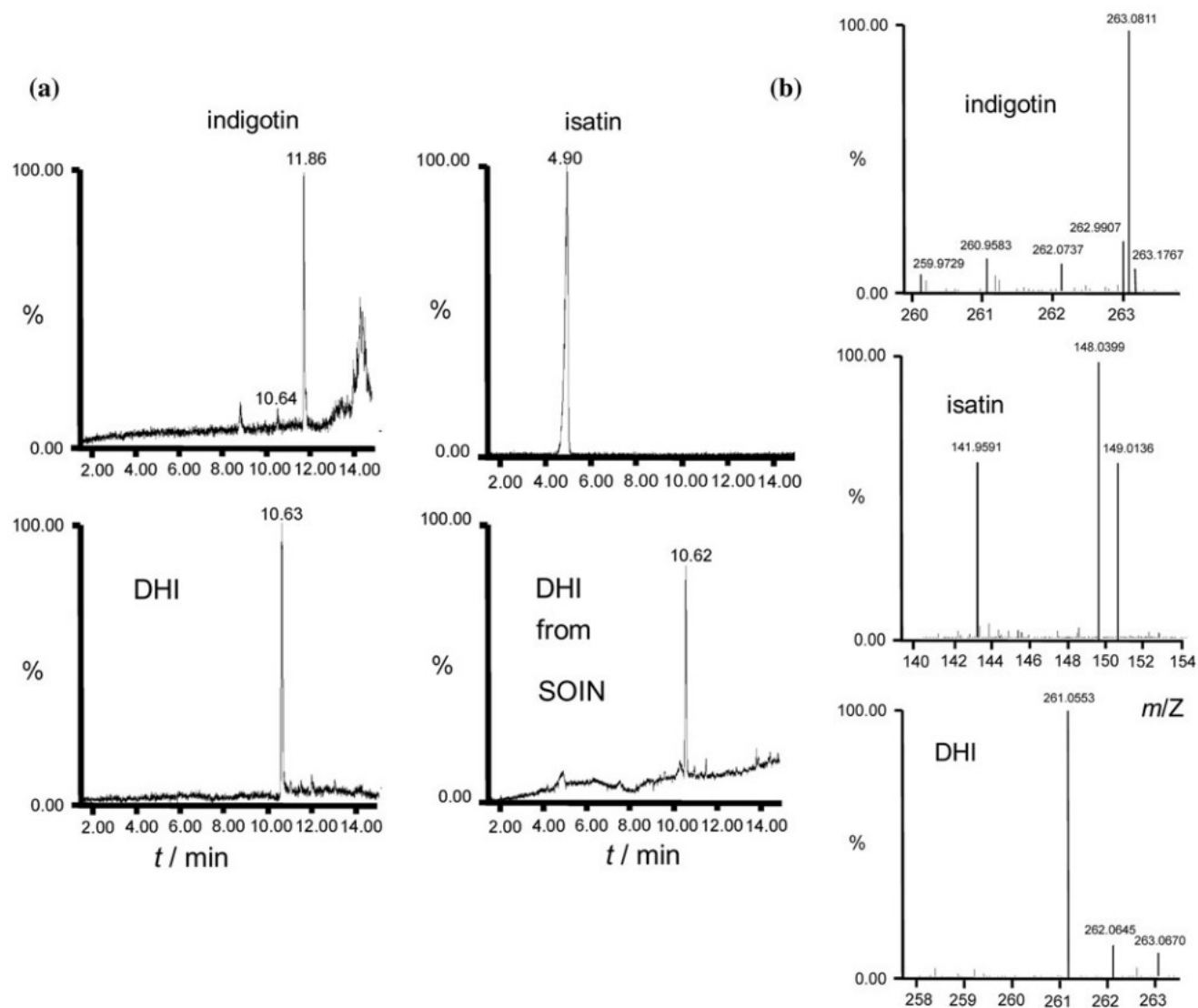


Fig. 5 **a** UPLC-MS of different DMSO extracts; **b** mass spectra of indigo (t_r 11.9 min), isatin (t_r 4.9 min), and dehydroindigo (t_r 10.6 min), recorded during the above UPLC-MS experiments

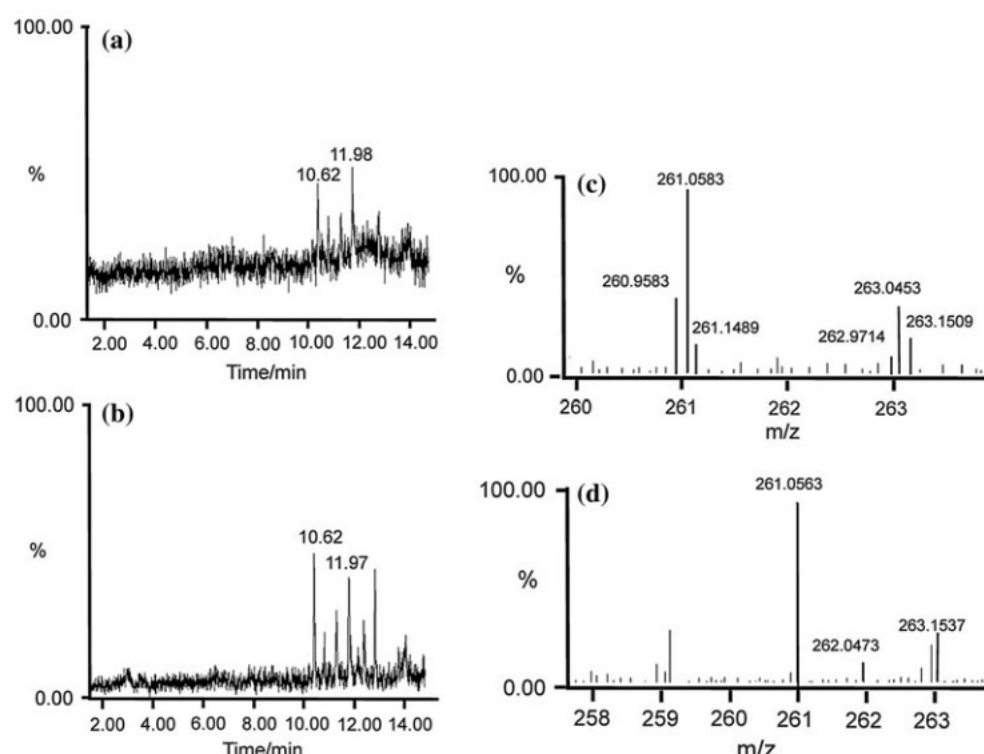
Table 2 Target compounds in the extracts samples and their corresponding $[M+H]^+$ values detected by HRMS (ionization mode: ESI+) in UPLC-MS experiments

Compound	t_R (min)	$[M+H]^+$ (m/z) detected	$[M+H]^+$ (m/z) isotopic model	Deviation (ppm)
Isatin	4.85	148.0393	148.0387	4.1
Dehydroindigo	10.62	261.0582	261.0664	[10.0
Indigo	11.89	263.0821	263.0815	2.3

[55, 70]. The reduced product is soluble, so that the electron transfer process is followed by dimerization to form isatide, reduced electrochemically at slightly more negative potentials [55, 70], so that the reduction peak appears as enhanced. The main reduction process for the reduction of isatin is accompanied by indigo-characteristic signals at +0.45 and -0.30 V, denoting that indigo appears as a ubiquitous component of almost all samples of indigoids. Conversely, the isatin-localized reduction peak at -0.55 V

also appears in the voltammograms of indigo (Fig. 7a). Remarkably, the voltammogram for commercial ‘Maya Blue’ (IN@K, Fig. 7c) shows the indigo peaks accompanied from isatin signal, similarly to the SOIN sample (Fig. 7d). In this sample, however, the peak at +0.45 V, corresponding to the oxidation of indigo to dehydroindigo, is almost entirely absent. These features are consistent with the aforementioned coexistence of isatin, dehydroindigo, and indigo in such samples. Taking into account that indigo

Fig. 6 UPLC–MS chromatograms for samples: **a** IN@K, **b** IN@P₁₅₀; and mass spectra in the region of molecular ions for: **c** indigo (*t*_r 11.9 min) and **d** dehydroindigo (*t*_r 10.6 min) recorded in chromatograms of IN@K and IN@P₁₅₀



and dehydroindigo produce the same voltammetric peaks at +0.45 and –0.30 V, the unique difference between them should be the relative height of such peaks. Consistently, the voltammograms for IN@K, IN@P_t, and SOIN samples exhibit peak current ratios between voltammetric peaks at +0.45 and –0.30 V clearly differing from those measured for indigo. These results indicate that the dehydroindigo/indigo ratio can be estimated from the relative height of the above voltammetric peaks.

Thermochemical calculations and in-depth dye distribution

The above data denote that a significant proportion of dehydroindigo accompanies indigo (and other minority components) in the extracts from MB-type specimens. Such extracts represent the fraction of externally adsorbed dye, but one can expect that, on increasing the temperature of the thermal treatment, the fraction of dye entering into the palygorskite pore/channel system increases. Chromatographic data agree well with these expectancies. As can be seen in Fig. 8, where LC–DAD chromatograms for DMSO extracts of specimens IN@P₁₂₀ and IN@P₁₆₀ are shown, the dehydroindigo/indigo ratio increases on increasing temperature, while the total area of the chromatographic peaks decreases. This means that the amount of extractable dye decreases on increasing temperature.

An estimate of thermochemical parameters can be made on assuming that the composition of the extracts was

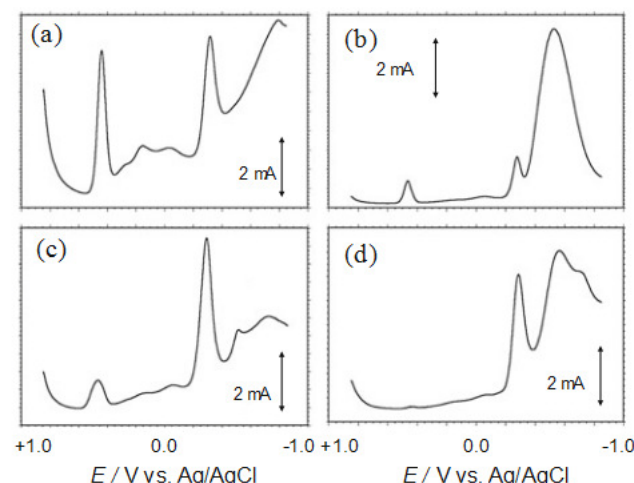
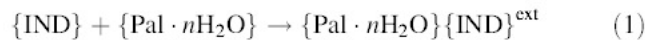


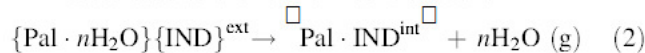
Fig. 7 Square wave voltammograms for paraffin-impregnated graphite electrodes modified with: **a** indigo, **b** isatin, **c** sample IN@K, **d** sample SOIN in contact with aqueous 0.50 M HAc/NaAc, pH 4.75. Potential scan initiated at +0.85 V in the negative direction. Potential step increment 4 mV; square wave amplitude 25 mV; frequency 5 Hz

representative of the composition of the externally adsorbed dye molecules when an equilibrium-like situation was reached. To perform thermochemical calculations, the attachment of indigo and dehydroindigo to palygorskite using the usual crushing plus heating treatment can be represented by the following sequence of processes (see thermochemical cyclic scheme in Fig. 9):

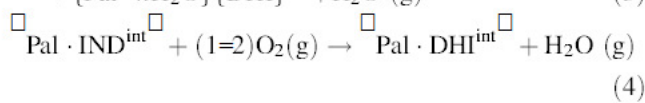
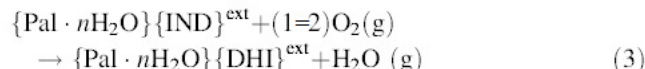
- (a) Disaggregation of indigo grains to yield indigo molecules externally attached to the hydrated palygorskite support:



- (b) Formation of a strong indigo–palygorskite complex associated to the loss of zeolitic water:



Additionally, we assume that the indigo to dehydroindigo oxidation process can occur in both the ‘external’ and ‘internal’ dye–clay complexes (notice that the terms ‘internal’ and ‘external’ are used as an oversimplification, for brevity):



Chromatographic peak area for dehydroindigo and indigo peaks (see Fig. 8) are representative of DMSO extractable, externally adsorbed molecules. Experimental data reveal that the total area of such peaks decreases on increasing the temperature of thermal treatment while the dehydroindigo/indigo ratio increases as a result of the parallel conversion of indigo into dehydroindigo. Although, under our experimental conditions, the requisites for

reaching chemical equilibrium in closed systems are not strictly accomplished, an apparent equilibrium constant for the process described by Eq. (3), $K_3(\text{IND})^{\text{app}}$, could be estimated at each temperature T , by the relationship:

$$K_3^{\text{app}} = \mathbf{n} \frac{A_T(\text{DHI})}{A_T(\text{IND})} \quad (5)$$

where $A_T(\text{DHI})$ and $A_T(\text{IND})$ denote, respectively, the area of the dehydroindigo and indigo peaks in the chromatogram of the DMSO extract of the sample prepared at temperature T , and \mathbf{n} represents a chromatographic coefficient of response to convert peak areas into relative concentrations whose value, determined from chromatograms of indigo and dehydroindigo solutions of known concentration was estimated close to one (0.98) under the used chromatographic conditions. The variation of $K_3(\text{IND})^{\text{app}}$ with the temperature should follow the Van’t Hoff law; i.e., a linear variation of $\ln K_3(\text{IND})^{\text{app}}$ on $1/T$ whose slope equals to $DH_3^{\circ}(\text{IND})^{\text{app}}/R$. Data in Fig. 10a reveal a reasonable linearity, allowing for an estimate of $DH_3^{\circ \text{app}} = (+72.6 \pm 1.5) \text{ kJ/mol}$. The similarity of this value with that calculated for the binding energy of water to palygorskite (66.5 kJ/mol) [13] suggests that the formation of dehydroindigo, even in the external regions of palygorskite, could be related to the loss of zeolitic water. Neglecting the dehydroindigo contribution between 100 and 140 °C (see data in Fig. 10b), one can approach the value of the apparent equilibrium constant for reaction (2), using the relationship:

$$K_2(\text{IND})^{\text{app}} \approx \frac{A_0(\text{IND})}{A_T(\text{IND})} \frac{A_T(\text{IND})}{A_T(\text{DHI})} \quad (6)$$

where $A_0(\text{IND})$ denotes the peak area of the indigo peak for the specimen prepared by crushing indigo and palygorskite at room temperature. Experimental data (Fig. 10a) yield a linear variation of $\ln K_2(\text{IND})^{\text{app}}$ on $1/T$ leading to

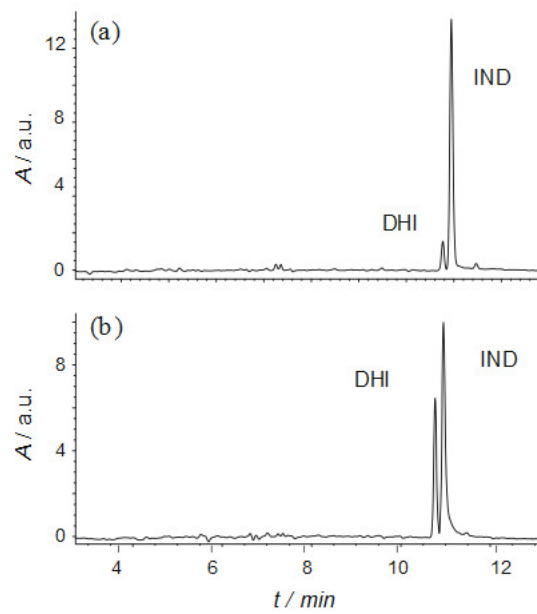


Fig. 8 LC–DAD for DMSO extracts of MB-type samples **a** IN@P₁₂₀ and **b** IN@P₁₆₀ specimens using the chromatographic conditions described in “Experimental” section

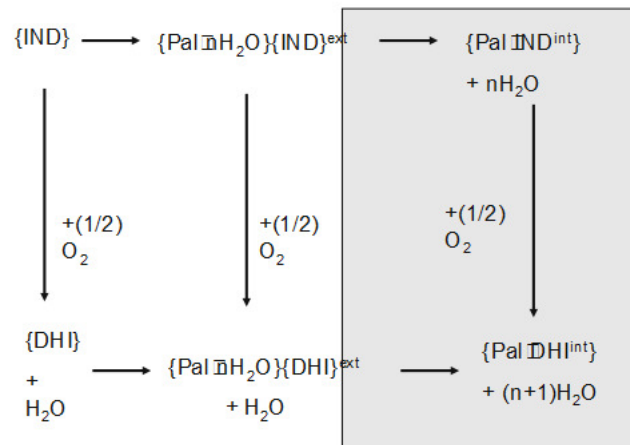


Fig. 9 Thermochemical cycle for processes involved in the indigo and dehydroindigo attachment to palygorskite clay

$DH_2^\circ(\text{IND})^{\text{app}} = (+43.8 \pm 0.9)$ kJ/mol. Similarly, the fraction of ‘internal’ (indigo plus dehydroindigo) dye relative to the total dye, f_{ext} , can be estimated on assuming that, for non-heated specimens, all the indigo (with none dehydroindigo) remains externally adsorbed to the clay, using the relationship:

$$f_{\text{ext}} = \frac{A_0(\text{IND}) - A_T(\text{IND})}{A_0(\text{IND})} = \frac{nA_T(\text{DHI})}{A_0(\text{IND})} \quad (7)$$

Chromatographic data suggest that, above 100 °C, the proportion of dye strongly attached to the palygorskite framework is large, increasing slowly with temperature, as can be seen in Fig. 10b. Data for $\{\text{Pal}\cdot n\text{H}_2\text{O}\}\{\text{DHI}\}^{\text{ext}}/\{\text{Pal}\cdot n\text{H}_2\text{O}\}\{\text{IND}\}^{\text{ext}}$ in this figure reveal that this ratio increases monotonically with temperature. Such values can be correlated with the dehydroindigo/indigo ratios calculated from square wave voltammetric data using the methodology previously described to evaluate the molar

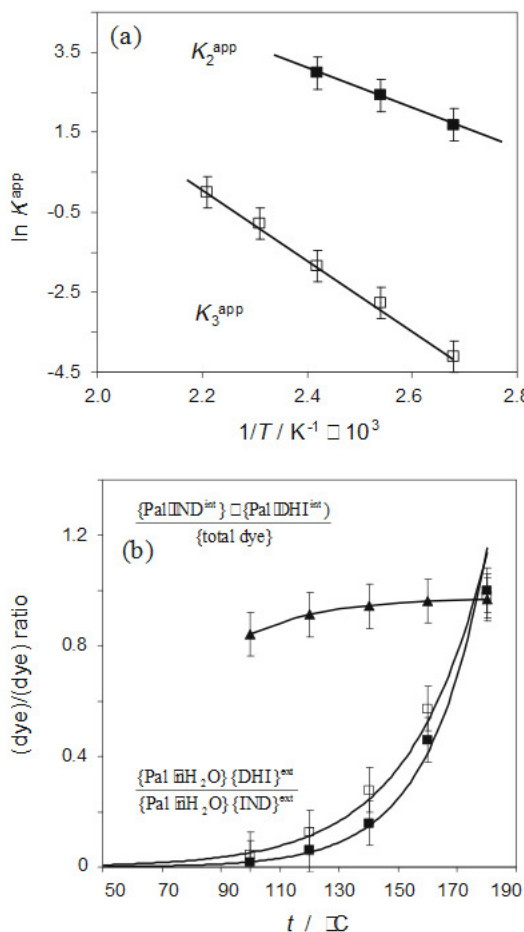


Fig. 10 **a** Van’t Hoff plots of $\ln K_{2\text{app}}$ and $\ln K_{3\text{app}}$ versus $1/T$ from chromatographic data. **b** Temperature dependence of the (total ‘internal’ dye)/(total dye) ratio (solid triangles) and the $\{\text{Pal}\cdot n\text{H}_2\text{O}\}\{\text{DHI}\}^{\text{ext}}/\{\text{Pal}\cdot n\text{H}_2\text{O}\}\{\text{IND}\}^{\text{ext}}$ ratio estimated independently from chromatographic (solid squares) and SWVs (squares) such as in Fig. 7, square wave frequency 50 Hz

fraction of the oxidized form of a depolarizer existing in its oxidized and reduced forms [71], taking into account that, depending on the experimentation time, voltammograms are representative of the average dye composition more or less deeply placed in the palygorskite crystals [32–38, 53]. Data represented in Fig. 10b correspond to the dehydroindigo/indigo ratios calculated from SWVs at a square wave frequency of 50 Hz. Such data, which can be taken as representative of the dye composition in external palygorskite layers, provide an excellent agreement with regard to the variation of the $\{\text{Pal}\cdot n\text{H}_2\text{O}\}\{\text{DHI}\}^{\text{ext}}/\{\text{Pal}\cdot n\text{H}_2\text{O}\}\{\text{IND}\}^{\text{ext}}$ ratio with the temperature of thermal treatment calculated from independent chromatographic data.

Implications for MB studies

The results presented here provide a confirmation of our previous reports introducing dehydroindigo as a dyeing component accompanying indigo in MB [32–37]. It is pertinent to underline, however, the difficulty in detecting its presence in MB samples due to the low amount of the organic fraction (ca. 1 wt%) in the indigo-dye complex, increased by the fact that dehydroindigo is a minor component relative to indigo. Then, it is not surprising that dehydroindigo spectral features were not detected in indigo plus palygorskite specimens prepared from high indigo loadings (until 20 wt%) in recent reports by Sánchez del Río et al. [26] and Tsiantos et al. [41], largely exceeding the theoretical maximum (ca. 4 wt%) of indigo loadings able to be stored within the palygorskite channels [52]. It is pertinent to note that, such specimens, strictly, cannot be considered as MB samples, as far as the peculiar, characteristic properties of the pigment are not completely accomplished.

Current data indicate, additionally, that other minor components, such as isatin and indirubin appear in MB-type samples. Remarkably, the presence of oxidized compounds (at least in significant proportion) requires the application of heating treatments, a commonly accepted requisite for preparing MB [9–27]. This implies that, dehydroindigo (but most likely other minor components) can be considered as an essential component defining the composition of MB. In fact, the role of dehydroindigo as a chromatic contributor to MB hue is important [32–37]. This is illustrated from the diffuse reflectance spectra of indigo and isatin reference products, the “soft-oxidation” prepared dehydroindigo (SOIN) and the MB-type specimen IN@P₁₈₀, shown in Fig. 11. These spectra confirm the results obtained in the extraction/LC experiments. As it can be seen in this figure, dehydroindigo and isatin spectral features are detected in the spectrum of MB-type samples. Interestingly, these features are absent (or almost entirely

absent) in the spectra of indigo plus palygorskite specimens which have not been submitted to thermal treatment. It should be noted that, strictly, these results indicate the presence of dehydroindigo in the extractable fraction of synthetic MB-type specimens. As far as thermal treatment of indigo plus palygorskite mixtures is needed for the generation of significant amounts of dehydroindigo, it is reasonable to assume that dehydroindigo-associated to palygorskite should exists in genuine MB. This is supported by spectral and voltammetric data on synthetic specimens and genuine MB samples [32–37]. The current results support the idea that, apart from bathochromic shift of indigo absorption bands as a result of the dye attachment to the clay support, the variable dehydroindigo/indigo proportion, presumably resulting from different thermal treatment, contributes significantly to the peculiar variability in the color of MB [32–35]. Then, the role of the palygorskite support would be to provide, via partial dehydration, the reaction medium appropriate for obtaining the oxidized forms of indigo. No significant isatin peaks were obtained under such extraction/chromatography conditions, thus suggesting that palygorskite acts, to some extent, as a template favoring the oxidation of indigo to dehydroindigo rather than the subsequent oxidation to isatin.

It should be emphasized, however, that several unexplained questions on MB remain. These are focused on the existing coordinative arrangement(s) and the location(s) of the different dye molecules to the palygorskite support. Previous kinetic data [53] suggest that the formation process of MB-type materials proceeds via two consecutive reactions, the first one consisting of the loss of zeolitic water of the palygorskite coupled with clay-indigo attachment and partial indigo to dehydroindigo oxidation, the second step possibly consisting of the diffusion-controlled penetration of the different dye molecules in the palygorskite channel system. The multicomponent nature of

MB provides a complex view of that system as a polyfunctional organic–inorganic hybrid material where the identification, distribution, coordination, and functionality of different components (including minor organic components but also metal ions) has to be elucidated by future research.

Conclusions

Extracts from synthetic MB specimens, including one commercial formulation, obtained upon treatment with organic solvents, permits to detect unambiguously the presence of dehydroindigo and other organic compounds such as isatin and indirubin as minority component accompanying indigo in such formulations, on the basis of their spectral and voltammetric signatures and mass spectrum from UPLC–MS experiments. The formation of dehydroindigo, isatin, and other minority components would result from the oxidation of indigo favored by its attachment to the palygorskite clay, the formation of such oxidized products being prompted by the application of thermal treatments. These results confirm our previous reports [32–35] introducing this new component, dehydroindigo, into the MB scenario and its concomitant importance to interpret the peculiar hue variability of the pigment as well as for describing the MB as a polyfunctional inorganic–organic hybrid material.

Acknowledgements Financial support is gratefully acknowledged from the MICINN Projects CTQ2011-28079-C03-01 and 02 which are also supported with ERDF funds.

References

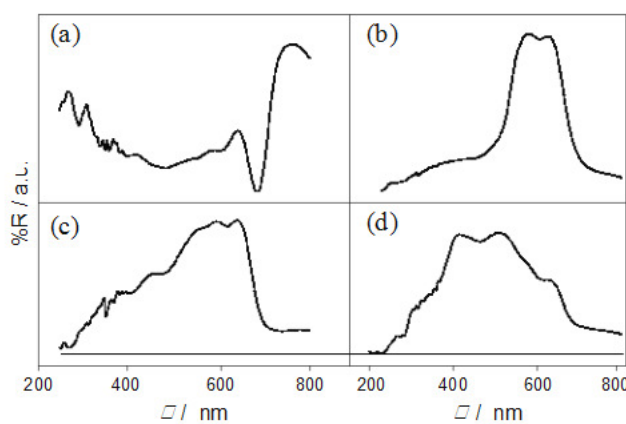


Fig. 11 Diffuse reflectance spectra of samples of reference products (a) indigo, (b) isatin, (c) SOIN sample, and (d) IN@P₁₅₀ sample

1. Merwin HE (1931) In: Morris HE, Charlton J, Morris AA (eds) Yucatan, Temple Warriors at Chichen Itza. Carnegie Institution, Washington, DC, p 356
2. Gettens RJ, Stout GL (eds) (1946) Paint materials: a short encyclopedia. Van Nostrand, New York
3. Reyes-Valerio C (1993) De Bonampak al Templo Mayor: el azul Maya en Mesoamérica. Siglo XXI, México
4. Romero P, Sánchez C (2005) New J Chem 29:57
5. Shepard AO (1962) Am Antiq 27:565
6. Gettens RJ (1962) Am Antiq 27:557
7. Van Olphen H (1967) Science 154:645
8. Cooksey CJ (2012) Biotech Histochem 87:439
9. Kleber R, Masschelein-Kleiner R, Thissen J (1967) Stud Conservat 12:41
10. José-Yacamán M, Rendón L, Arenas J, Serra-Puche MC (1996) Science 273:223
11. Fernández ME, Ascencio JA, Mendoza-Anaya D, Rodríguez-Lugo V, José-Yacamán M (1999) J Mater Sci 34:5243. doi: [10.1023/A:1004724316051](https://doi.org/10.1023/A:1004724316051)
12. Polette LA, Meitzner G, José-Yacamán M, Chianelli RR (2002) Microchem J 71:167
13. Chiari G, Giustetto R, Ricchiardi G (2003) Eur J Mineral 15:21

14. Hubbard B, Kuang W, Moser A, Facey GA, Detellier C (2003) *Clays Clay Miner* 51:318
15. Fois E, Gamba A, Tilocca A (2003) *Microporous Mesoporous Mater* 57:263
16. Reinen D, Köhl P, Müller C (2004) *Zeich Anorg Allgem Chem* 630:97
17. Sánchez del Río M, Martinetto P, Somogyi A, Reyes-Valerio C, Dooryhee E, Peltier N, Alianelli L, Moignard B, Pichon L, Caligaro T, Dran J-C (2004) *Spectrochim Acta B* 59:1619
18. Sánchez del Rio M, Sodo A, Eeckhout SG, Neisius T, Martinetto P, Dooryhee E, Reyes-Valerio C (2005) *Nucl Instrum Methods Phys Res B* 238:50
19. Giustetto R, Llabres i Xamena FX, Ricchiardi G, Bordiga S, Damin A, Gobetto R, Chierotti MR (2005) *J Phys Chem B* 109:19360
20. Chianelli RR, Perez De la Rosa M, Meitzner G, Siadati M, Berhault G, Mehta A (2005) *J Synchrotron Radiat* 12:129
21. Manciu FS, Reza L, Polette LA, Torres B, Chianelli RR (2007) *J Raman Spectrosc* 38:1193
22. Polette-Niewold LA, Manciu FS, Torres B, Alvarado M, Chianelli RR (2007) *J Inorg Biochem* 101:1958
23. Fuentes ME, Peña B, Contreras C, Montero AL, Chianelli R, Alvarado M, Olivas R, Rodríguez LM, Camacho H, Montero-Cabrera LA (2008) *Int J Quantum Chem* 108:1664
24. Chiari G, Giustetto R, Družik J, Doehe E, Ricchiardi G (2008) *Appl Phys A* 90:3
25. Tilocca A, Fois E (2009) *J Phys Chem C* 113:8683
26. Sánchez del Río M, Boccaleri E, Milanesio M, Croce G, van Beek W, Tsiantos C (2009) *J Mater Sci* 44:5524. doi: [10.1007/s10853-009-3772-5](https://doi.org/10.1007/s10853-009-3772-5)
27. Sánchez del Río M, Doménech A, Doménech MT, Vázquez ML, Suárez M, García-Romero E (2011) *Dev Clay Sci* 3:453
28. Mondelli C, Sanchez del Rio M, Gonzalez MA, Magazzù A, Cavalleri C, Suárez M, García-Romero E, Romano P (2012) *J Phys Conf Ser* 340:012109
29. Scholz F, Meyer B (1998) In: Bard AJ, Rubinstein I (eds) *Electroanalytical chemistry. A series of advances*, vol 20. Marcel Dekker, New York, p 1
30. Scholz F, Schröder U, Gulabowski R (2005) *Electrochemistry of immobilized particles and droplets*. Springer, Berlin
31. Doménech A, Labuda J, Scholz F (2013) *Pure Appl Chem* 85:609
32. Doménech A, Doménech MT, Vázquez ML (2006) *J Phys Chem B* 110:6027
33. Doménech A, Doménech MT, Vázquez ML (2007) *J Phys Chem C* 111:4585
34. Doménech A, Doménech MT, Vázquez ML (2007) *Anal Chem* 79:2812
35. Doménech A, Doménech MT, Vázquez ML (2009) *Archaeometry* 51:1015
36. Doménech A, Doménech MT, Sánchez del Río M, Goberna S, Lima E (2009) *J Phys Chem C* 113:12118
37. Doménech A, Doménech MT, Sánchez del Río M, Vázquez ML (2009) *J Solid State Electrochem* 13:869
38. Doménech A (2010) *Electrochemistry of porous materials*. Taylor & Francis, Boca Raton
39. Rondao R, De Melo JS, Bonifacio BD, Melo M (2010) *J Phys Chem A* 114:1699
40. Giustetto R, Seenivasan K, Bonino F, Ricchiardi G, Bordiga S, Chierotti MR, Gobetto R (2011) *J Phys Chem C* 115:16764
41. Tsiantos C, Tsampodimou M, Kacandes GH, Sánchez del Río M, Gionis V, Chrysikkos GD (2012) *J Mater Sci* 47:3415. doi: [10.1007/s10853-011-6189-x](https://doi.org/10.1007/s10853-011-6189-x)
42. Lima E, Guzmán A, Vera M, Rivera JL, Fraissard J (2012) *J Phys Chem C* 116:4556
43. Sanz E, Arteaga A, García MA, Cámaras C, Dietz C (2012) *J Archaeol Sci* 39:3516
44. Doménech A, Doménech MT, Sánchez del Río M, Vázquez ML, Lima E (2009) *New J Chem* 33:2371
45. Vandebaele P, Bodé S, Alonso A, Moens L (2005) *Spectrochim Acta A* 61:2349
46. Doménech A, Doménech MT, Vázquez ML (2011) *Angew Chem Int Ed* 50:5741
47. Doménech A, Doménech MT, Vidal C, Vázquez ML (2012) *Angew Chem Int Ed* 51:700
48. Giustetto R, Seenivasan K, Pellerej D, Ricchiardi G, Bordiga S (2012) *Microporous Mesoporous Mater* 155:167
49. Kalb L (1909) *Ber Dtsch Chem Ges* 42:3642
50. Klessinger M, Lüttke W (1963) *Tetrahedron* 19(Suppl 2):315
51. Hein M, Phuong NTB, Michalik D, Görsls H, Lalk M, Langer P (2006) *Tetrahedron Lett* 47:5741
52. Yasarawan N, van Duijneveldt JS (2008) *Langmuir* 24:7184
53. Doménech A, Doménech M, Osete L, Montoya N (2013) *Microporous Mesoporous Mater* 2013(166):123
54. Perpéte EA, Preat J, André J-M, Jacquemin D (2006) *J Phys Chem A* 110:5629
55. Diculescu VC, Kumbhat S, Oliveira-Brett AM (2006) *Anal Chim Acta* 575:190
56. Wille E, Lüttke W (1973) *Chem Ber* 106:3240
57. Seixas de Melo J, Moura AP, Melo MJ (2004) *J Phys Chem A* 108:6975
58. Tatsch E, Schrader B (1995) *J Raman Spectrosc* 26:467
59. Sánchez del Río M, Picquart M, Haro-Poniatowski E, van Elslande E, Uc VH (2006) *J Raman Spectrosc* 37:1046
60. Tomkinson J, Bacci M, Picollo M, Colognesi D (2009) *Vib Spectrosc* 50:268
61. Brunel JL, Lassegues JC, Sourisseau C (2002) *J Raman Spectrosc* 33:815
62. Zheng W, Angelopoulos M, Epstein AJ, MacDiarmid AG (1997) *Macromolecules* 30:2953
63. Trchova M, Stejskal J, Prokes J (1999) *Synth Met* 101:840
64. Iwan A, Kaczmareczyk B, Janeczek H, Sek D, Ostrowski S (2007) *Spectrochim Acta A* 66:1030
65. Fabbri D, Chiavari G, Ling H (2000) *J Anal Appl Pyrolysis* 56:167
66. Chiavari G, Fabbri D, Prati S, Zappi A (2005) *Chromatographia* 61:403
67. Casas MJ, Doménech MT (2005) *Anal Bional Chem* 382:259
68. Gross JH (2004) *Mass spectrometry*. Springer, Berlin
69. Doménech A, Doménech MT, Vázquez ML (2007) *J Solid State Electrochem* 11:1335
70. He JB, Ma G-H, Chen J-C, Yao Y, Wang Y (2010) *Electrochim Acta* 55:4845
71. Doménech A, Martini M, De Carvalho L, Doménech MT (2012) *J Electroanal Chem* 684:13